



CELLULAR AND MOLECULAR BIOLOGY

An Efficient Synthesis of Novel Dextran-Arsenite Nanoparticles intended for Potential Antitumor Drug Material

WEIBING LAN, SHAN CHEN & GUANGZAI NONG

Abstract: The functionalization of polysaccharides with synthetic nanopolymers has attracted great attention owing to the applications of this method in many industrial fields. This work aimed to investigate the effect of arsenic trioxide on the functionalization of dextran. Dextran-arsenite nanoparticle formation was induced by microwave with sulfuric acid as a catalyst. Various analytical techniques were used to verify the structure of the nanopolymers. Besides, various reaction conditions, such as dextran concentration, arsenic trioxide concentration and pH, were investigated to determine their impact on particle size. The results indicated that the product was an arsenite-based nanomaterial retaining the basic configuration of dextran and that the product size was positively correlated with pH but negatively correlated with arsenic trioxide concentration. Moreover, the inhibitory effects of the dextran-arsenite nanoparticles on the growth of the human colorectal cancer cell line HCT-116 and human hepatoma carcinoma cell lines Huh-7 and SMMC-7721 were studied. The results showed that the product could inhibit the proliferation of these three tumor cell lines in a dose-dependent manner. Therefore, the product could be a new type of functional nanomaterial for further study on the synthesis, biological activity and development of polysaccharide drugs.

Key words: Antitumor activity, arsenic trioxide, nanopolysaccharides, nanoparticles.

INTRODUCTION

Tumors are currently a global problem, and in recent decades, the incidence of tumors has been high. Treatment with drugs such as porphyrin (Batinic-Haberle et al. 2018), docetaxel (Baal et al. 2018) and oxaliplatin (Ganot et al. 2018) is generally used. However, this treatment modality suffers from problems such as poor water solubility, poor stability, high cost and complicated production, which lead to limitations on bioavailability and clinical application. These problems also result in a shortage of drugs. Therefore, the development of more antitumor drugs or antitumor drug-based materials is urgently needed.

The development of new drugs and drug materials based on polysaccharides has always been a key area of concern (Mansur et al. 2018). Dextran (DEX) is commonly modified to expand its function due to its advantages, such as its abundance, simple preparation, biocompatibility and biodegradability (Guoming & Mao 2012). There are reports on the sulfuration, carboxymethylation, derivatization with biradical groups, sulfonylation and phosphorylation of DEX. However, as far as we know, few studies have reported the arsenic acidification of DEX. Therefore, to solve the problems of the shortage of antitumor drugs and antitumor drug-based materials and the high cost of DEX and to enhance the medicinal value of DEX, the

modification of DEX with arsenic trioxide (ATO, As_2O_3) was pursued.

ATO is effective against solid malignant tumors (Glorieux & Calderon 2018). However, the bioavailability and bioactivity of ATO are greatly limited because of the narrow margin between its functional threshold and toxicity (Kong et al. 2014). Preparation of ATO into various micro- and nanoparticles (Liu et al. 2016) and conversion into other organoarsenic compounds are ways to reduce its side effects (Saha et al. 1999). Moreover, our group has found that sucrose and ATO can produce sucrose arsenite, which can inhibit tumor cell activity and reduce the toxic side effects of ATO (See Figure S1 - Supplementary Material). However, to the best of our knowledge, few studies have reported the use of DEX and ATO to prepare a dextran-arsenite nanocomposite, including its synthetic mechanism and an evaluation of its antitumor activity. Moreover, the feasibility of controlling the size of this nanocomposite by adjusting parameters was given to increase attention (Skalickova et al. 2016).

In this study, DEX-ATO nanomaterials from DEX and ATO were synthesized by sulfuric acid catalysis using a microwave heating method. The DEX-ATO nanoparticles were characterized, and the factors affecting their size were investigated. Besides, to analyze its potential as a therapeutic agent for cancer treatment, the antitumor properties of the product were evaluated. The research can provide a theoretical basis for the development of new antitumor materials.

MATERIALS AND METHODS

Materials

DEX standards with Mw values of 0.667, 5.90, 11.80, 2.28, 4.73, 1.12×10^2 , 2.12×10^2 , 4.04×10^2 , 7.78×10^2 , and 2×10^3 kDa were obtained from Polymer Laboratories Ltd. (USA). DEX (Mw =10 kDa) was

purchased from Ye Source Biotechnology Ltd. (China). The human colorectal cancer cell line (HCT-116), human hepatoma carcinoma cell line (Huh-7) and human hepatoma carcinoma cell line (SMMC-7721) were obtained from the Shanghai Cell Bank of the Chinese Academy of Sciences (China).

Synthesis of DEX-ATO nanoparticles

DEX-ATO nanoparticles were synthesized by the microwave-induced free radical polymerization method. Briefly, a DEX solution (500 mg/ml) was prepared by dissolving DEX in ultrapure water under stirring at room temperature. The DEX solution was diluted with ultrapure water to obtain different concentrations. Next, ATO solutions with various concentrations were slowly added to the DEX solution with mild stirring (400 rpm), and then 0.1 M sulfuric acid solution was added to adjust the pH. The mixed solution was transferred to a reaction vessel and placed in a microwave oven (Milestone, USA) with a temperature probe, as shown in Figure 1. Microwave irradiation was performed for 30 min. Finally, the solution was further heated to 170°C by an electric oven in 30 min. Then, the resulting solution was cooled to room temperature and filtered to remove residue. The filtrate was placed in a dialysis membrane bag for 36 h. Finally, lyophilization was performed to obtain the DEX-ATO nanoparticles.

Characteristic measurements

To verify the structure of the DEX-ATO nanoparticles, UV-Vis absorption spectra were collected from 200 nm to 800 nm by a Shimadzu UV-2501 UV spectrophotometer (Japan) (Dopp et al. 2010, Rana 2018). Fourier transform infrared (FTIR) spectra were obtained on a Tensor II FTIR spectrophotometer (Bruker, Germany) with a resolution of 1/cm and 16 scans in the range of 4,000-400/cm (Liu et al. 2018). 1H

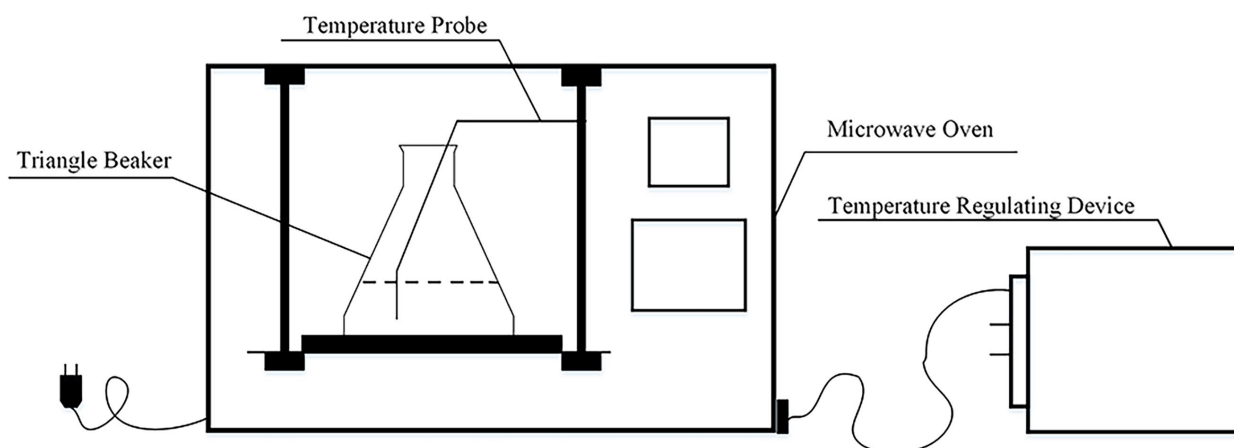


Figure 1. Equipment drawing.

NMR and ^{13}C NMR spectra were obtained on an NMR spectrophotometer (Bruker, Switzerland) operating at a frequency of 600 MHz using D_2O as the solvent (Chen et al. 2018, Mario et al. 2015). A differential scanning calorimeter (DSC) Q2000 (TA Instruments, US) was used to obtain a thermal characteristic curve at a scanning heating rate of $10^\circ\text{C}/\text{min}$ from 30°C to 350°C .

The High-performance gel permeation chromatography (HPGPC) was performed on an Agilent 1100 HPGPC system with three Shodex Sugar columns (KS-801, KS-805 and KS-Guard) in series, and an Agilent G1362A differential refraction detector. The column temperature was maintained at $65 \pm 1^\circ\text{C}$, and the eluent was ultra-pure water at a flow rate of $1.0\text{ ml}/\text{min}$. The standards were DEX (Huang et al. 2018).

To further confirm the structure of the DEX-ATO nanoparticles, high-performance liquid chromatography-mass spectrometry (HPLC-MS) was used. The DEX-ATO nanocomposite was dissolved with acetonitrile to obtain a $1\text{ }\mu\text{g}/\text{ml}$ sample solution. The equipment model and chromatographic column used for the chromatography experiment were an I-CLASS UPLC system (Waters Corp., US) and an ACQUITY UPLC BEH C18 column (Waters, $2.1\text{ mm}\times 50\text{ mm}$, $1.7\text{ }\mu\text{m}$), respectively. The mobile phase consisted of (A) 0.1% methanoic acid in water and (B)

acetonitrile. The elution conditions were as follows: 0–5 min, 40% B; 5–20 min, 40–70% B; 20–30 min, 70–95% B; 30–40 min, 95% B. The flow rate was $0.5\text{ ml}/\text{min}$. The column was maintained at 25°C . MS analysis was carried out by a XEVOG2-XSQ-TOF mass spectrometer (Waters, US) with an electrospray ionization source in positive-ion mode according to the method of Schipper et al. (2017) with some modifications. The capillary voltage was 3000 V. The source temperature and desolvation temperature were 100 and 450°C , respectively. The flow rates of the trap gas and desolvation gas were 0.012 and $640\text{ L}/\text{h}$, respectively. The mass range (m/z) was 50–2000.

SEM was performed on a Hitachi SU8220 FESEM (Hitachi Limited, Japan) with a 0.05% concentration (wt %) of sample drawn onto tin foil and then dried.

Particle size measurements were performed on a Zetasizer Nano ZS90 instrument (Malvern Instruments, UK).

Antitumor activity

The antitumor activity of the tested sample was evaluated in HCT-116, Huh-7 and SMMC-7721 according to Gomha's method (Gomha et al. 2015). McCoy's 5A medium was used for incubating the HCT-116 cells, and DMEM was used for incubating the Huh-7 cells and SMMC-7721

cells. The medium was supplemented with 10% fetal bovine serum, phosphate-buffered saline (PBS) and 50 µg/ml-penicillin streptomycin solution. The propagated cells were maintained at 37 °C in a humidified atmosphere with 5% CO₂. For the antimicrobial activity assay, the cells were seeded in 100 µL of growth medium in 96-well plates at a cell concentration of 2×10⁴ cells/ml. After 24 h of seeding, fresh medium containing different concentrations of the tested sample with water as the solvent was added to the previously seeded cells. Serial dilutions of the tested samples were added to confluent cell monolayers dispersed in the 96-well plates, which were incubated for 24 h in a humidified incubator at 37 °C with 5% CO₂. Three wells were used for each tested sample concentration. Control cells were incubated without the polymeric sample. After incubation of the cells, tested polymeric samples at various concentrations were added, and the incubation was continued for 24 h at 37 °C. The cell viability was determined by a colorimetric method. All experiments were carried out in triplicate. The IC₅₀ value was calculated using Origin 9.0 software with a logistic model.

Statistical analysis

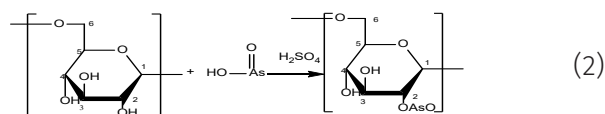
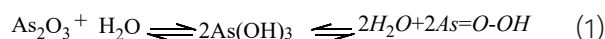
All experiments were performed in triplicate and analyzed as the mean ± standard deviation. The experimental data were analyzed by SPSS 11.0 software (SPSS Inc., Chicago, IL, USA) and plotted by Origin 9.0 (Origin Lab Corp., USA).

RESULTS AND DISCUSSION

Synthesis mechanism

The reaction pathway for the synthesis of DEX-ATO is considered, as shown in formulas 1 and 2. First, ATO is dissolved in water and converted into arsenic tri-hydroxide As(OH)₃ and then arsenic acid (Ralph 2008). Second, DEX is

positively charged under acidic conditions and forms DEX-ATO with arsenic acid under sulfuric acid catalysis (Stewart et al. 1999). Since the hydroxyl groups attached to the DEX sugar ring are secondary, they are highly sterically hindered and cannot rotate freely in the spatial conformation of DEX, resulting in poor reactivity. Also, the order of reactivity of the secondary hydroxyl groups on the sugar ring is C2-OH>C3-OH>C4-OH. Therefore, the 2-hydroxyl group has the advantage over the hydroxyl groups at the 3- and 4-positions of being able to contact arsenic acid to form an arsenite group.



Characterization analysis

To determine whether arsenic interacted with the hydroxyl groups and was converted into an organoarsenic compound, UV and FTIR spectroscopy were used. NMR, DSC, HPGPC, SEM and HPLC-MS were also used for characterization. The results are shown in Figure 2, Figure 3 and Figure 4. As shown in Figure 2a, the absorbance peak of DEX-ATO was located at 283 nm, which indicated that As was connected to DEX to form an -organoarsenic compound (Kiranmayi et al. 2015).

As shown in Figure 2b, the bands in the FTIR spectra of DEX-ATO are similar to bands in the DEX spectrum, including those corresponding to the OH, CH₂, CH, C-O-C, C-C-O, C-C-C and pyran groups (Goretti Llamas-Arriba et al. 2019). However, two new bands at 1273.53 and 842.33 cm⁻¹ appeared, corresponding to the ATO stretching and bending vibrations, respectively (Sritham & Gunasekaran 2017). Furthermore the absorption peaks of -OH is shifted towards

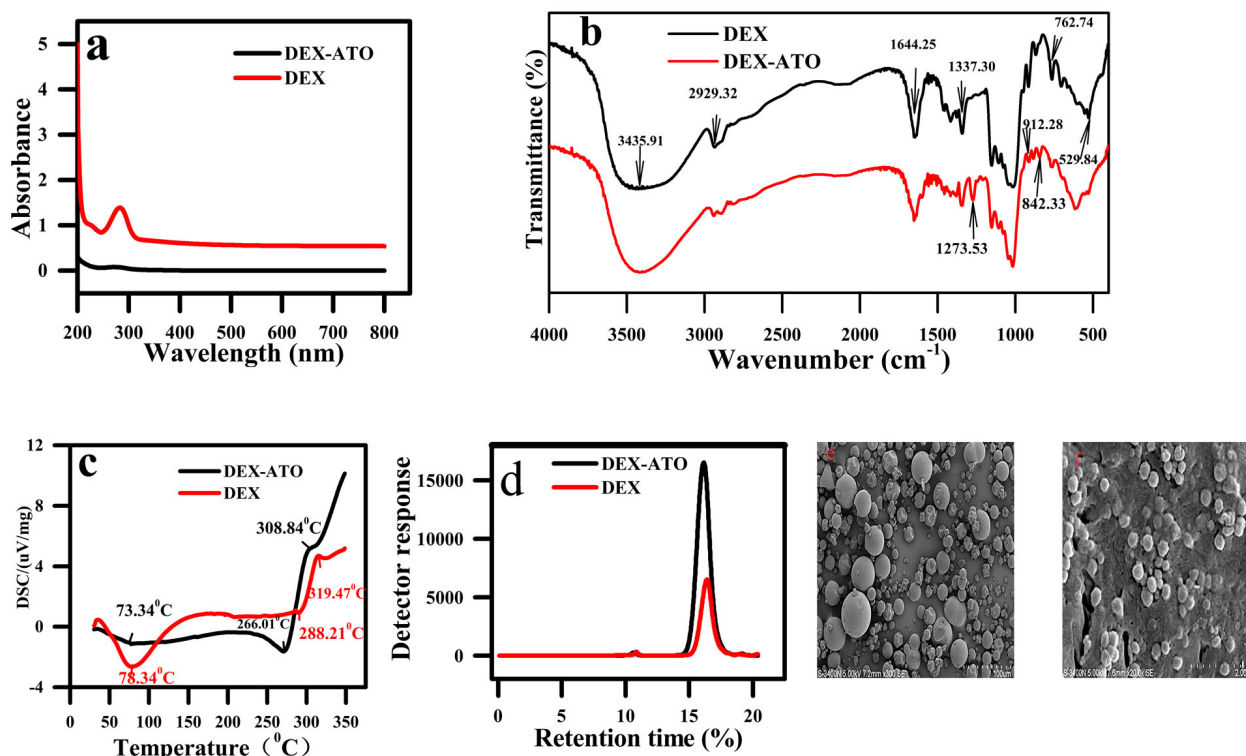


Figure 2. Structural characterization of DEX and DEX-ATO. (a) UV; (b) FTIR; (c) DSC; (d) HPGPC; (e) SEM of DEX; (f) SEM of DEX-ATO.

lower wavenumbers, which confirmed the strong interaction between ATO and DEX. These results led to the conclusion that a rapid combination of ATO occurred at a high temperature because of the $-OH$ groups of DEX and that the basic structure of DEX remained unchanged.

The 1H and ^{13}C NMR spectra are shown in Figure 3. The anomeric proton peak at δ 4.87 ppm in the 1H NMR spectrum was attributed to the glycosidic protons involved in the α -(1-6) linkages (Gomha et al. 2015), which was in good agreement with the presence of an FTIR absorption peak at δ 912.28 cm^{-1} . The peaks at δ 3.89, 3.82, 3.66, 3.48 and 3.42 ppm corresponded to H5, H6, H3, H2 and H4, respectively. The anomeric carbon signal was assigned to the peak at δ 97.64 ppm, which confirmed that the sugar residues were glycosidically linked (Du et al. 2018). The peaks at δ 73.31, 71.32, 69.43 and

70.09 ppm corresponded to C2, C3, C4, and C5, respectively (Mähner et al. 2001). In summary, the main structure of DEX was maintained in the DEX-ATO nanoparticles.

As shown in Figure 2c, the endothermic transition and exothermic transition of DEX-ATO appeared 73.34 and 308.84 $^{\circ}C$, respectively, which were lower than the corresponding transitions of DEX (78.34 and 391.47 $^{\circ}C$). This change can be attributed to the grafting of As-O groups onto backbone and the formation of free volume between branched chains upon grafting.

HPGPC spectra are shown in Figure 2d. The Mw of DEX-ATO was 1.03×10^4 Da, similar to the Mw of DEX. In the process of esterification, as the arsenite group combines with the hydrogen on the raw sugar chain, the Mw will increase. At the same time, because the reaction was carried out under strongly acidic conditions, some of the

sugar chains would degrade, causing the Mw to decline. The reason for the small change in the Mw of the DEX-ATO product might be because two factors had a similar degree of influence.

As shown in Figure 2e and 2f, SEM morphologies of the DEX and DEX-ATO nanoparticles revealed differences in their microstructures. These nanoparticles were spherical with little adhesion.

DEX-ATO was further analyzed by HPLC-MS concerning the product with a retention time of 5.215 min, and the results are shown in Figure 4. The main ion of DEX-ATO is the adduction ion at m/z 741.0561 ($[M+2H_2O+H]^+$). The chemical formula and simulation data are $C_{18}H_{39}As_2O_{21}$ and m/z 741.0410 respectively, which are assigned to $Gluc_3+2As(OH)_3+2H_2O+H$. The results indicated that the DEX ring structure had not changed. Combined NMR, HPGPC and FTIR, it leads to the conclusion that the basic structure of DEX was retained in the process of DEX-ATO synthesis.

Effect of different formulations on particle size

Particle size is one of the most significant determinants in the mucosal and epithelial tissue uptake of nanoparticles and the intracellular trafficking of particles (Panyam & Labhasetwar 2003). The effects of DEX concentration, ATO concentration and pH on the particle size of DEX-ATO nanoparticles are summarized in Table I. With an increase in DEX concentration in the range of 100-200 mg/ml, the particle size decreased linearly from 502 to 170 nm. This result can be explained by the fact that the DEX molecules with less concentrations have reacted completely and DEX does not play a role in steric stability. Additionally, due to the adjacent convergence of magnetic fields, naked ATO began to deposit based on the attraction between the two species. When the concentration of DEX was large enough, the particle size has clear trend since As-O bonds are formed on the macromolecular chains, causing the formation aggregates. However, when the ATO concentration increased from 2

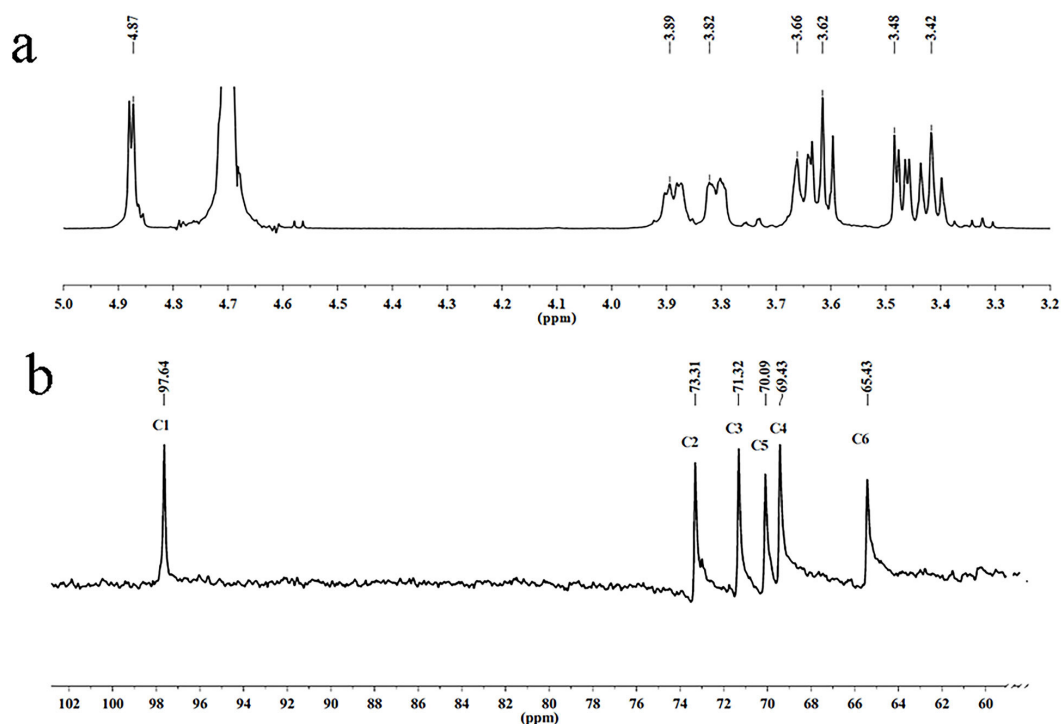


Figure 3. The NMR spectrum of DEX-ATO, a) is 1H spectrum, b) is ^{13}C spectrum.

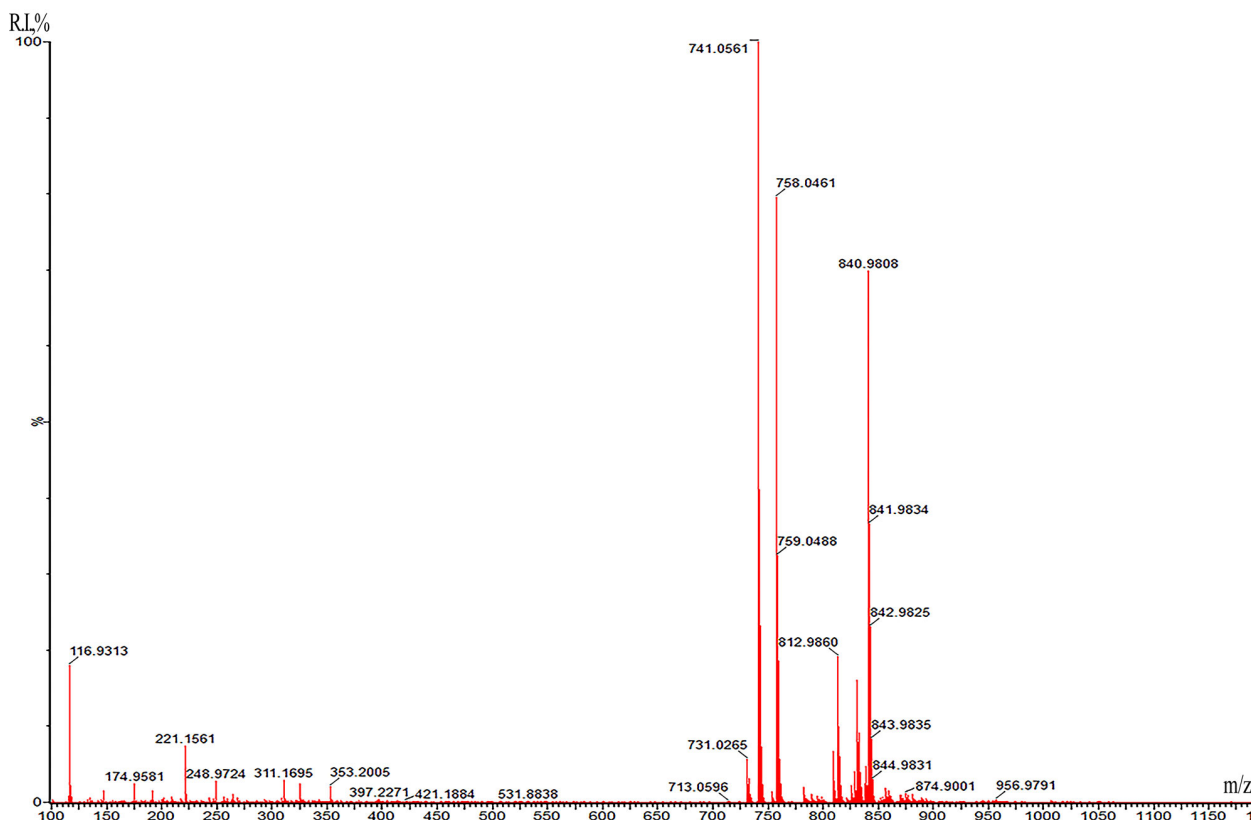


Figure 4. MS spectrum of the HPLC-MS analysis of the peak at 5.215 min.

Table I. The particle sizes of different formulations.

Nanoparticle	Particle size (nm)	Nanoparticles	Particle Size (nm)	Nanoparticles	Particle size (nm)
A1	502±5.32	B1	430±7.54	C1	135±4.39
A2	351±3.25	B2	410±6.44	C2	170±5.32
A3	170±3.35	B3	314±5.21	C3	238±4.64
A4	242±2.46	B4	258±6.38	C4	262±6.88
A5	341±8.29	B5	170±5.32		

Where, A1, A2, A3, A4 and A5 were the nanoparticle samples with DEX concentrations of 100, 150, 200, 250, and 300 mg/ml respectively, when the ATO concentration and pH were 10 mg/ml and 3.5 respectively. B1, B2, B3, B4, and B5 were the nanoparticles samples with ATO concentrations of 2, 4, 6, 8, and 10 mg/ml respectively, when the DEX concentration and pH were 100 mg/ml and 3.5 respectively. C1, C2, C3 and C4 were the nanoparticle samples with pH of 2.5, 3.5, 4.5 and 5.5 respectively, when the DEX concentration and ATO concentration were 100 mg/ml and 10 mg/ml respectively. The values were expressed as mean ± standard error.

to 10 mg/ml, the particle size decreased slightly from 430 to 170 nm. These trends were following previously reported results (Hong et al. 2008). Besides, the particle size increased linearly from 135 to 262 nm with increasing pH in the range of 2.5–5.5 ($R^2 = 0.9686$). This could be explained by the fact that in an acidic medium, DEX will be positively charged, conferring a high charge density to the polysaccharide. Therefore, the surface charge density of the DEX molecules is strongly dependent on the solution pH (Ko et al. 2002), and the ionic cross-linking process for the formation of DEX-ATO nanoparticles is pH-dependent. Also, the increase in the measured average particle size when the solution pH increased could be caused mainly by particle aggregation, rather than by further growth of the individual particles after their initial formation (Gan et al. 2005). This result was consistent with the results of previous research (Ko et al. 2002).

Evaluation of the antitumor properties of the DEX-ATO nanoparticles

The antitumor activity of the samples was tested against three different cancer cell lines (HCT-116, Huh-7 and SMMC-7721), and the results are shown in Figure 5. OD values decreased with increasing DEX-ATO concentration, indicating that DEX-ATO had a strong inhibitory effect on the proliferation of these cells in vitro and had a selective and dose-dependent inhibitory effect on different cells. The reason was that the DEX modified with ATO interacted with the negatively charged cancer cells through electrostatic and H-bonding interactions (Erella et al. 2018). Moreover, based on a four-parameter logistic fitting, the IC₅₀ values of DEX-ATO were 254, 134 and 192 $\mu\text{g/ml}$ against HCT-116, Huh-7 and SMMC-7721 cells, respectively.

After 24 h of DEX-ATO treatment, the cell morphology is shown in Figure 6. The cells in the control group grew vigorously and densely, and

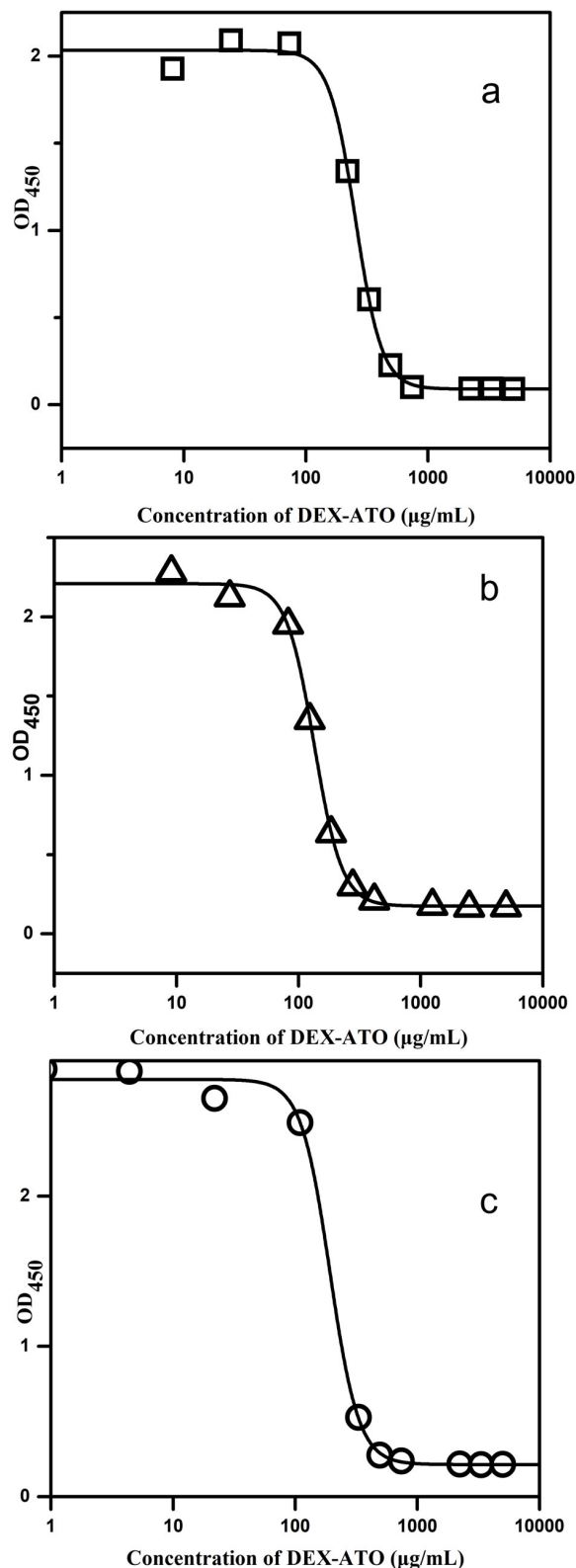


Figure 5. OD value curves of HCT-116(a), Huh-7(b) and SMMC-7721(c) cells as a function of the concentration of DEX-ATO.

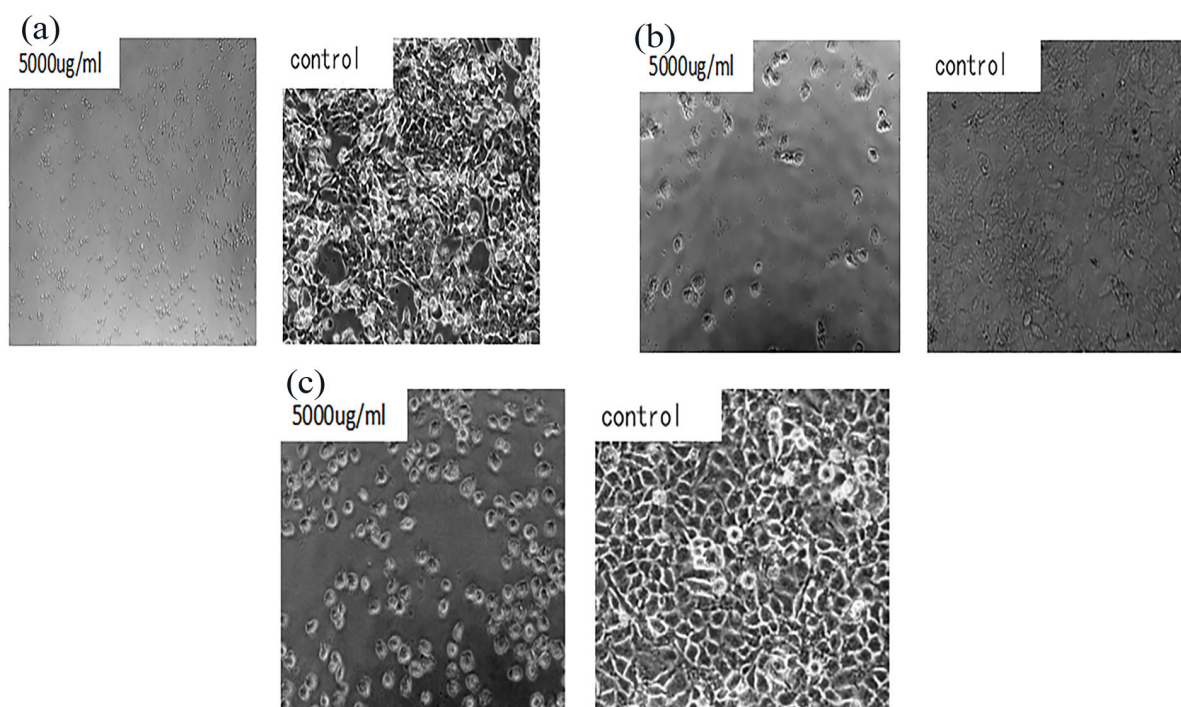


Figure 6. The cell morphology of HCT-116(a), Huh-7(b) and SMMC-7721(c) cells after 24 h of treatment.

the sizes of the cells were different. However, after DEX-ATO treatment, the morphologies of the HCT-116, Huh-7 and SMMC-7721 cells changed significantly, the number of cells significantly decreased, and the cells contracted into a circle, undergoing disintegration and necrosis. Therefore, DEX-ATO can induce apoptosis in HCT-116, Huh-7 and SMMC-7721 cells. This result was consistent with previous studies (Sadaf et al. 2018). It was further proven that DEX-ATO has an antitumor effect and was very likely to be used as a nanomaterial drug.

CONCLUSION

The present study demonstrated that DEX-ATO nanoparticles were synthesized via microwave thermal polymerization using sulfuric acid as a catalyst. The formation mechanism is that the hydroxyl group on the DEX molecule forms a chemical bond with arsenic acid. The particle

size can be modulated by controlling critical fabrication parameters, including the pH and DEX and ATO concentrations. Besides, DEX-ATO inhibits tumor cell growth and has a selective and concentration-dependent effect on tumor cells. Therefore, DEX-ATO not only may be able to prepare antitumor drugs independently, but also can be used as the basic material to prepare antitumor drugs. It is likely to be a new type of functional nanomaterials. However, DEX-ATO contains arsenic, so it is poisonous and may be a carcinogen. Hence, some basic studies should be performed before it is used as a legal drug, including toxicological experiments, drug metabolism and accumulation tests and process improvement studies. Moreover, there is a long way to go to further explore the role and mechanism of the product as an anticancer drug.

Acknowledgments

The authors express their thanks to the Engineering Center for Sugar and Comprehensive Utilization to the Sophisticated Instrument Laboratory of the University, and to teacher Xing Han, Wuhan University of Technology. The authors declare no conflict of interest.

REFERENCES

- BATINIC-HABERLE I, TOVMASYAN A & SPASOJEVIC I. 2018. Mn porphyrin-based redox-active drugs - Differential effects as cancer therapeutics and protectors of normal tissue against oxidative injury. *Antioxid Redox Signal* 29: 1691-1724.
- BRAAL CL, DE BRUIJN P, ATRAFI F, VAN GEIJN M, RIJCKEN CJF, MATHIJSSSEN RHJ & KOOLEN SLW. 2018. A new method for the determination of total and released docetaxel from docetaxel-entrapped core-crosslinked polymeric micelles by LC-MS/MS and its clinical application in plasma and tissues in patients with various tumours. *J Pharm BiomeAnal* 161: 168-174.
- CHEN Y, WU D, ZHONG W, KUANG S, LUO Q, SONG L, HE L, FENG X & TAO X. 2018. Evaluation of the PEG Density in the PEGylated Chitosan Nanoparticles as a Drug Carrier for Curcumin and Mitoxantrone. *Nanomaterials* 8: 486-501.
- DOPP E, KLIGERMAN AD & DIAZ-BONE RA. 2010. Organoarsenicals. Uptake, metabolism, and toxicity. *Met Ions Life Sci* 7: 231-265.
- DU R, QIAO X, ZHAO F, SONG Q, ZHOU Q, WANG Y, PAN L, HANY & ZHOU Z. 2018. Purification, characterization and antioxidant activity of dextran produced by *Leuconostoc pseudomesenteroides* from homemade wine. *Carbohydr Polym* 198.
- ELELLA MHA, MOHAMED RR & SABAA MW. 2018. Synthesis of novel grafted hyaluronic acid with antitumor activity. *Carbohydr Polym* 189: 107-114.
- GAN Q, WANG T, COCHRANE C & MCCARRON P. 2005. Modulation of surface charge, particle size and morphological properties of chitosan-TPP nanoparticles intended for gene delivery. *Colloid Surf B-Biointerfaces* 44: 65-73.
- GANOT N, BRIAITBARD O, GAMMAL A, TAM J, HOCHMAN J & TSHUVA EY. 2018. In Vivo Anticancer Activity of a Nontoxic Inert Phenolato Titanium Complex: High Efficacy on Solid Tumors Alone and Combined with Platinum Drugs. *Chem Med Chem* 13(21): 2290-2296.
- GLORIEUX C & CALDERON PB. 2018. Catalase down-regulation in cancer cells exposed to arsenic trioxide is involved in their increased sensitivity to a pro-oxidant treatment. *Cancer Cell Int* 18(1): 24.
- GOMHA SM, EL-HASHASH MA, EDREES MM & EL-ARAB EE. 2015. Synthesis, Characterization, and Molecular Docking of Novel bis-thiazolyl Thienothiophene Derivatives as Promising Cytotoxic Antitumor Drug. *Molecules* 21: 1-17.
- GORETTI LLAMAS-ARRIBA M, PUERTAS AI, PRIETO A, LOPEZ P, COBOS M, MIRANDA JJ, MARIETA C, RUAS-MADIEDO P & TERESA DUENAS M. 2019. Characterization of dextrans produced by *Lactobacillus mali* CUPV271 and *Leuconostoc carnosum* CUPV411. *Food Hydrocolloids* 89: 613-622.
- GUOMING S & MAO JJ. 2012. Engineering dextran-based scaffolds for drug delivery and tissue repair. *Nanomedicine* 7(11): 1771-1784.
- HONG RY, FENG B, CHEN LL, LIU GH, LI HZ, ZHENG Y & WEI DG. 2008. Synthesis, characterization and MRI application of dextran-coated Fe₃O₄ magnetic nanoparticles. *Biochem Eng J* 42(3): 290-300.
- HUANG Y, WU X, ZHOU S, LIN Y, ZHANG W, FU C, LUO L, WANG K, XIE X & FAN H. 2018. Biphasic extraction of different polysaccharides from *Radix Sophorae Tonkinensis* by microwave-assisted aqueous two-phase extraction: process optimization, structural characterization and mechanism exploration. *Sep Purif Technol* 207: 187-198.
- KIRANMAYI PM, ASOK A & LEE B. 2015. Organoarsenicals in poultry litter: detection, fate, and toxicity. *Environ Int* 75: 68-80.
- KO JA, PARK HJ, HWANG SJ, PARK JB & LEE JS. 2002. Preparation and characterization of chitosan microparticles intended for controlled drug delivery. *Int J Pharm* 249: 165-174.
- KONG H, YANG J, ZHANG Y, FANG Y, NISHINARI K & PHILLIPS GO. 2014. Synthesis and antioxidant properties of gum arabic-stabilized selenium nanoparticles. *Int J Biol Macromol* 65: 155-162.
- LIU H, ZHANG Z, CHI X, ZHAO Z, HUANG D, JIN J & GAO J. 2016. Arsenite-loaded nanoparticles inhibit PARP-1 to overcome multidrug resistance in hepatocellular carcinoma cells. *Sci Rep* 6: 31009.
- LIU Z, LI X, ZHAN P, HU F & YE X. 2018. Removal of cadmium and copper from water by a magnetic adsorbent of PFM: Adsorption performance and micro-structural morphology. *Sep Purif Technol* 206: 199-207.
- MÄHNER C, LECHNER MD & NORDMEIER E. 2001. Synthesis and characterisation of dextran and pullulan sulphate. *Carbohydr Res* 331(2): 203-208.
- MANSUR AAP, CARVALHO SM, LOBATO ZIP, LEITE MD, CUNHA AD & MANSUR HS. 2018. Design and Development of

Polysaccharide-Doxorubicin-Peptide Bioconjugates for Dual Synergistic Effects of Integrin-Targeted and Cell-Penetrating Peptides for Cancer Chemotherapy. *Bioconjugate Chem* 29(6): 1973-2000.

MARIO F, PETERSEN JF, HANSEN JS & CHRISTENSEN JRB. 2015. Guest-Host Chemistry with Dendrimers-Binding of Carboxylates in Aqueous Solution. *PLoS ONE* 10: e0138706.

PANYAM J & LABHASETWAR V. 2003. Biodegradable nanoparticles for drug and gene delivery to cells and tissue. *Adv Drug Deliv Rev* 55: 329-347.

RALPH SJ. 2008. Arsenic-based antineoplastic drugs and their mechanisms of action. *Met Based Drugs* 1: 260146.

RANA AKN, TYAGI M & JAGADEVAN S. 2018. Leaf-extract mediated zero-valent iron for oxidation of Arsenic (III): Preparation, characterization and kinetics. *Chem Eng J* 347: 91-100.

SADAF N, KUMAR N, ALI M, ALI V, BIMAL S & HAQUE R. 2018. Arsenic trioxide induces apoptosis and inhibits the growth of human liver cancer cells. *Life Sci* 205: 9-17.

SAHA JC, DIKSHIT AK, BANDYOPADHYAY M & SAHA KC. 1999. A Review of Arsenic Poisoning and its Effects on Human Health. *C R C Critical Reviews in Environmental Control* 29(3): 281-313.

SCHIPPER DA, LOUIS AV, DICKEN DS, JOHNSON K, SMOLENSKI RT, BLACK SM, RUNYAN, R, KONHILAS J, GARCIA JGN & KHALPEY Z. 2017. Improved metabolism and redox state with a novel preservation solution: implications for donor lungs after cardiac death (DCD). *Pulm Circ* 7: 494-504.

SKALICKOVA S, MILOSAVLJEVIC V, CIHALOVA K, HORKY P, RICHTERA L & ADAM V. 2016. Selenium nanoparticles as a nutritional supplement. *Nutrition* 33.

SRITHAM E & GUNASEKARAN S. 2017. FTIR spectroscopic evaluation of sucrose-maltodextrin-sodium citrate bioglass. *Food Hydrocolloids* 70: 371-382.

STEWART MS, SPALLHOLZ JE, NELDNER KH & PENCE BC. 1999. Selenium compounds have disparate abilities to impose oxidative stress and induce apoptosis. *Free Radic Biol Med* 26: 42-48.

SUPPLEMENTARY MATERIAL

Figure S1. OD value curve of HCT-116(a), Huh-7(b) and SMMC-7721(c) cells on the function of the concentration of the product.

How to cite

LAN W, CHEN S & NONG G. 2021. An Efficient Synthesis of Novel Dextran-Arsenite Nanoparticles intended for Potential Antitumor Drug Material. *An Acad Bras Cienc* 93: e20190551. DOI 10.1590/0001-3765202120190551.

*Manuscript received on May 13, 2019;
accepted for publication on August 5, 2019*

WEIBING LAN^{1,2}

<https://orcid.org/0000-0003-0425-1221>

SHAN CHEN¹

<https://orcid.org/0000-0002-2621-4352>

GUANGZAI NONG¹

<https://orcid.org/0000-0001-5738-7793>

¹ Guangxi University, College of Light Industry and Food Engineering, No.100, Daxue East Road, Nanning, 530004, Guangxi, China

² Beibu Gulf University, College of Food Engineering, No.12, Binhai Avenue, Qinzhou 535011, China

Correspondence to: **Shan Chen/ Guangzai Nong**

E-mail: chen-shann@foxmail.com/ gznonginguilin@163.com

Author contributions

Weibing Lan performed the antioxidant, antimicrobial and immunological assays, as well as writing the manuscript. Shan Chen helped with the experimental design and writing of the manuscript. Guangzai Nong performed the structural and phytochemical analyses.

